communications chemistry

A Nature Portfolio journal

Article

https://doi.org/10.1038/s42004-025-01650-8

Supramolecular chiral inversion and regulation of phenylalanine-based organogels in low-polarity achiral solvents

Wannian Zhang [1,2], Fang Yu[1,3] & Yu-Peng He [1,2]

Metamaterials with supramolecular chirality have been widely developed in many fields, and their assembly modes provide valuable insights for understanding living systems. In this work, we achieved for the first time the inversion of supramolecular chirality in organogels using a low-polarity achiral solvent. Furthermore, the regulation of supramolecular chirality was achieved through structural modification of the achiral moieties. Additionally, the impact of hydrogen bond variability on the modulation of supramolecular chirality was investigated by replacing the O atom with the N atom. Subsequently, the mechanisms governing supramolecular chirality modulation through low-polarity solvents and weakly polar structural motifs was elucidated. The results demonstrate that weak-polarity solvents, achiral long-chain moieties, and hydrogen bonds can individually serve as effective modulators for regulating intermolecular assembly patterns, thereby exerting critical influence on the emergence of supramolecular chirality. These findings establish a robust foundation for the precise construction and manipulation of supramolecular chirality in organogel systems.

Supramolecular chiral organogels have garnered increasing attention due to their potential applications in chiroptical switching[1–6], sensor devices[2,4,5,7,8], and circularly polarized luminescence[9,10]. To enhance their practical applicability, effective regulation of supramolecular chirality in organogels becomes imperative[1,11–22]. Current strategies for chirality modulation in organogel systems are primarily categorized into two approaches: chiral factor-based regulation and achiral factor-mediated regulation[23]. The chiral factor-based approach predominantly relies on modifying the intrinsic molecular chirality of gelators to manipulate supramolecular chirality[24–30], typically governed by the majority rule[31–35] and sergeant-and-soldiers rule[32,36–39]. Although extensively investigated in supramolecular chirality research, however, this strategy requires either altering the intrinsic chiral configuration of gelators or introducing additional chiral moieties, which has dramatically complicated the flexible chirality modulation. In contrast, achiral factor-mediated regulation circumvents the need for modifying molecular chiral configuration, transcending the conventional limitations of chiral factor-based regulation and offering more flexible, cost-effective, and efficient strategies[4,40–42]. Consequently, achiral factor-driven modulation of supramolecular chirality in organogels has recently emerged as a burgeoning research frontier[43–45].

Recent advancements have witnessed growing reports on achiral factor-mediated regulation of supramolecular chirality in gel systems. Notably, the Liu group pioneered chiral modulation through structural modification of gelator side chains[46]. Zhao and co-workers achieved supramolecular chirality inversion via coordination with transition metal ions[47,48]. Subsequent investigations by Liu et al. revealed time-dependent chirality switching in gel systems[49]. More systematic studies have demonstrated chirality manipulation through variations in achiral segments within gelator design, collectively establishing fundamental mechanisms for supramolecular chirality control[3,50,51]. Current research in this field predominantly focuses on solvent polarity effects for chirality regulation. However, the potential of weak polarity solvent engineering in manipulating supramolecular gel chirality remains largely unexplored[52,53], presenting a critical knowledge gap in achiral modulation strategies.

In this work, a series of phenylalanine-derived organogelators (*L*-PheO$_n$) capable of supramolecular chirality inversion in low-polarity achiral solvents. A systematic approach was implemented to explore chirality modulation mechanisms (Fig. 1). Initially, a simple solvent shift from weakly polar solvents, such as *n*-octane to cyclohexane, successfully inverted supramolecular chirality without structural modification of gelators. Subsequently, the modulation of supramolecular chirality was similarly achieved by modification of the achiral tail chain of *L*-PheO$_n$(Fig. 1a). To elucidate hydrogen bonds effects on chiral expression, amide-functionalized analogs (*L*-PheN$_n$) were synthesized by replacing ester linkages with

[1]State Key Laboratory of Fine Chemicals, Ningbo Institute of Dalian University of Technology, Ningbo, China. [2]School of Chemical Engineering, Dalian University of Technology, No.2 Linggong Road, Dalian, China. [3]College of Pharmaceutical Engineering and Biotechnology, College of Cosmetics, Zhejiang Pharmaceutical University, No 666 Siming Road, Ningbo, China. e-mail: yupeng.he@dlut.edu.cn

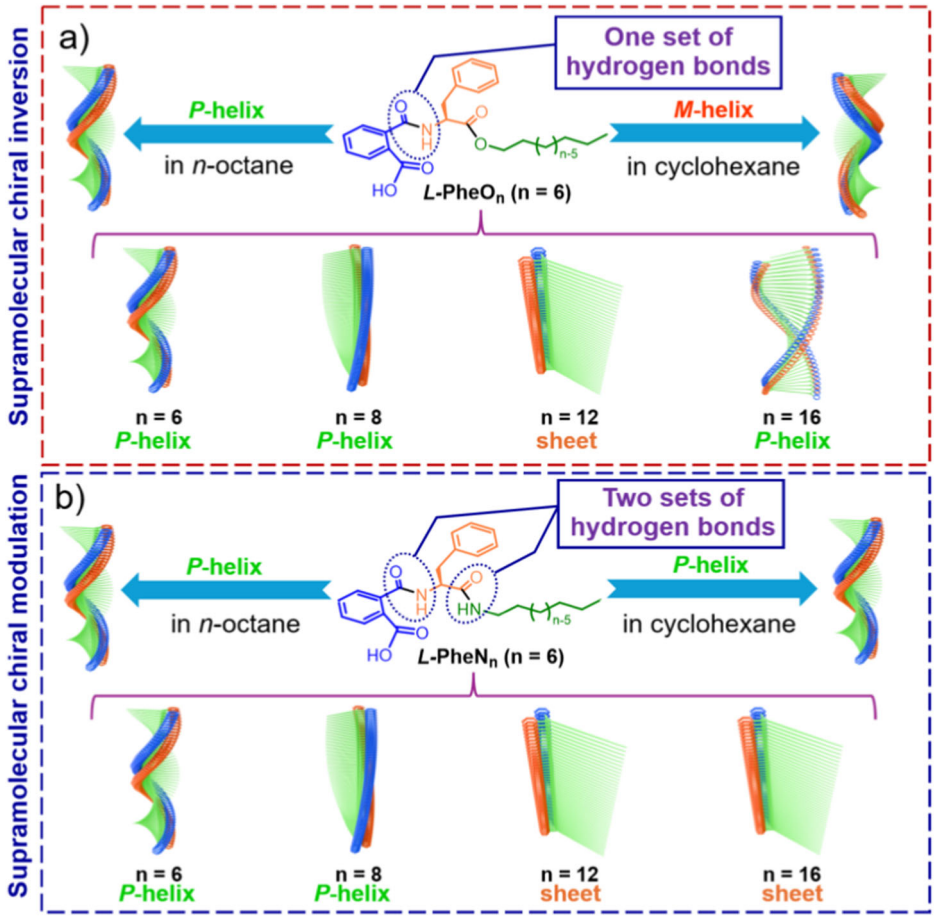

Fig. 1 | Supramolecular chiral inversion and regulation of organogelators in achiral alkane solvents driven by hydrogen bond interactions. **a** Supramolecular chiral inversion of *L*-PheO$_n$ in low-polarity achiral solvent solvents, **b** Supramolecular chirality modulation of *L*-PheN$_n$ in low-polarity achiral solvent solvents.

stronger hydrogen bonds moieties. Enhanced intermolecular hydrogen bonds within gel assemblies were found to suppress chirality inversion (Fig. 1b). The above results demonstrate that all these achiral factors play a crucial role in the regulation of supramolecular chirality. Finally, to elucidate the assembly mode of this supramolecular gel, we conducted computational simulations on the supramolecular organogel system. Our findings demonstrate that the solvent environment, the length of the hydrophobic end chains, and hydrogen bond interactions critically govern the self-assembly behavior of the aggregates. These insights provide a foundation for the effective modulation of supramolecular gel chirality through achiral factors.

Results and discussion

Effect of low-polarity achiral solvents on supramolecular chirality

Supramolecular chirality of *L*-PheO$_6$ gels in two weakly polar solvents was initially characterized by SEM. In *n*-octane, *P*-helical chirality was shown (Fig. 2a), while in cyclohexane, *M*-helical chirality was shown (Fig. 2b). To elucidate the origin of this solvent-dependent chiral inversion, XRD analysis was employed to determine the possible structural arrangement of the organogel formed. The XRD profile of the cyclohexane gel of *L*-PheO$_6$ exhibited two broad peaks at 19.21° and 23.73° (Fig. 2e), which suggests that the form of assembly of *L*-PheO$_6$ in cyclohexane mainly relies on hydrogen bonds[54] and π-π stacking[45,55,56]. In contrast, the XRD spectrum of the *L*-PheO$_6$ in *n*-octane gel showed only hydrogen bonds (19.38°), and no π-π stacking interaction was clearly observed. This phenomenon may be attributed to the spatial structure effect of the *n*-octane solvent on the gel system. Specifically, the *n*-octane solvent likely hindered the formation of sufficient π-π stacking interactions within the *L*-PheO$_6$ gel aggregates, leading to an assembly pattern distinct from that observed in the *L*-PheO$_6$ cyclohexane gel and ultimately reversing the supramolecular chirality compared to the cyclohexane system.

To probe structural determinants of chiral modulation, an amide-functionalized analog (*L*-PheN$_6$, Fig. 2g) was synthesized. These analog features dual hydrogen bonds-capable amide moieties instead of ester groups in *L*-PheO$_6$, whereas the ester group in *L*-PheO$_6$ was not able to generate additional hydrogen bonds (Fig. 2g). SEM results showed that both cyclohexane gels and octane gels of *L*-PheN$_6$ exhibited the same *P*-helical chirality (Fig. 2c, d). XRD spectra revealed the absence of significant π-π stacking interactions in both the *n*-octane and cyclohexane gels of *L*-PheN$_6$, with only hydrogen bonds (19.87° and 19.62°) being observed. This contrasts sharply with the *P*-helical chirality of *L*-PheO$_6$ *n*-octane gels, which exhibit a similar interaction pattern dominated by hydrogen bonds. Based on these observations, we hypothesize that the inversion of supramolecular chirality is more readily achieved in *L*-PheO$_6$ gels due to their relatively limited hydrogen bond interactions, which render the assembly more susceptible to solvent-induced effects. The multiple hydrogen bonds in the *L*-PheN$_6$ molecule enhance polar interactions between gelator molecules while restricting the apolar interactions of other structural groups within *L*-PheN$_6$. This structural stabilization renders the aggregates less susceptible to solvent effects, thereby maintaining consistent helical chirality across two diverse weakly polar solvent systems.

Complementarily, FTIR spectroscopy was employed to characterize the hydrogen bonds evolution of both gelator systems in distinct solvent environments (Fig. 2f). The -NH and -CO vibrational modes of *L*-PheO$_6$ exhibited marked bathochromic shifts in distinct solvents, indicative of solvent-dependent hydrogen bonds reorganization. Notably, the *L*-PheO$_6$ cyclohexane gel exhibited -NH stretching vibrations at 3343 cm^{-1} with carbonyl (-CO) modes at 1736 and 1655 cm^{-1}. Conversely, its *n*-octane counterpart showed a bathochromic shift in -NH vibrations (3291 cm^{-1}) accompanied by altered carbonyl signatures (1734 and 1641 cm^{-1}) (Fig. 2f). This bathochromic evolution demonstrates enhanced hydrogen bonds strength in *L*-PheO$_6$ gel of *n*-octane[46]. In contrast, *L*-PheN$_6$ maintained

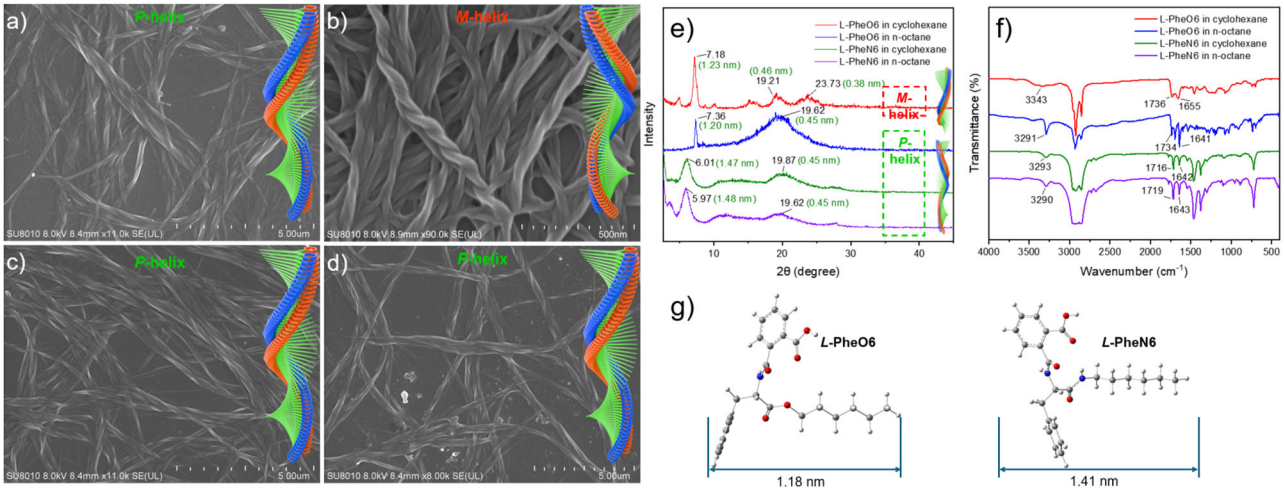

Fig. 2 | Assembly mechanism of organogels in *n*-octane and cyclohexane solvents. **a** SEM of *L*-$PheO_6$ in *n*-octane, **b** *L*-$PheO_6$ in cyclohexane, **c** *L*-$PheN_6$ in *n*-octane, **d** *L*-$PheN_6$ in cyclohexane, **e** XRD spectra of organogel, **f** FTIR spectra of organogel, **g** Geometric lengths of organogelators, which were obtained from the geometric conformation of the dimer with the lowest energy.

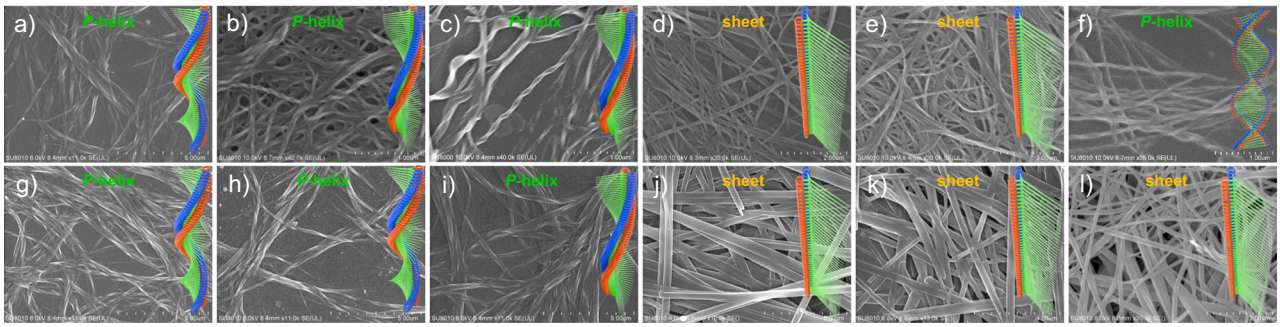

Fig. 3 | SEM of organogels in *n*-octane. **a** *L*-$PheO_6$, **b** *L*-$PheO_8$, **c** *L*-$PheO_{10}$, **d** *L*-$PheO_{12}$, **e** *L*-$PheO_{14}$, **f** *L*-$PheO_{16}$, **g** *L*-$PheN_6$, **h** *L*-$PheN_8$, **i** *L*-$PheN_{10}$, **j** *L*-$PheN_{12}$, **k** *L*-$PheN_{14}$, **l** *L*-$PheN_{16}$.

consistent vibrational signatures across both solvents, as NH at 3293 cm^{-1} in cyclohexane and 3290 cm^{-1} in *n*-octane, while carbonyl vibrations showed slight shifts from 1716 to 1719 cm^{-1} and from 1642 to 1643 cm^{-1}. Such spectral invariance suggests *L*-$PheN_6$ exhibits similar assembly behaviors in the two different solvents, distinct from the solvent-responsive behavior of *L*-$PheO_6$. This comparative analysis reveals that hydrogen bonds strength modulates the solvent adaptability of gelator assemblies in apolar solvents.

To elucidate the stereochemical influence of gelator architecture, the *D*-$PheO_6$ enantiomer was synthesized for comparative analysis of supramolecular chiral properties in the organogel. SEM analysis demonstrated inverted supramolecular helicity between *D*-$PheO_6$ and *L*-$PheO_6$, with the *D*-enantiomer adopting *M*-helical packing in *n*-octane versus *P*-helical organization in cyclohexane (Fig. S15). Spectroscopic evidence confirms that the dominant driven force during self-assembly of $PheO_6$ organogel is sensitive to solvent effect. One plausible hypothesis is that there is only single hydrogen bonds set in $PheO_6$, leading to chiral inversion in supramolecular architectures when processed in dissimilar low-polarity solvents. The enhanced hydrogen bond network as the self-assembly driving force for gelators enables the self-assembly behavior of $PheN_6$ aggregates to be less influenced by apolar solvents, while exhibiting identical supramolecular chirality in two distinct weakly polar solvents.

Effect of achiral tail chains on supramolecular chirality

Following the apolar solvent-mediated modulation of supramolecular chirality in organogels, we systematically examined the role of gelator hydrophobic chains in governing the chiral self-assembly of the gels. *L*-$PheO_n$ derivatives with n = 6, 8, and 10 alkyl chains formed *n*-octane-based organogels that displayed *P*-helical supramolecular chirality, as evidenced in Fig. 3a–c. Notably, supramolecular chirality was abolished upon alkyl chain elongation to $n = 12$ and 14 (Fig. 3d, e). It is hypothesized that the van der Waals interaction between gelators and solvents was enhanced with increasing hydrophobic tail chain length of gelators, which critically disrupts the orientation of intermolecular hydrogen bonds and leads to the disappearance of supramolecular helical chirality. Intriguingly, upon increasing the hydrophobic chain length to $n = 16$ (Fig. 3f), the gel exhibited a re-emergence of *P*-helix supramolecular chirality.

Subsequently, *L*-$PheN_n$ and *L*-$PheO_n$ were retained for comparative analysis to elucidate structural determinants of chiral assembly. The *L*-$PheN_n$/*n*-octane gel exhibits *P*-helical supramolecular chirality at chain lengths $n = 6, 8, 10$ (Fig. 3g–i), with complete chiral disruption emerging at $n = 12, 14$ (Fig. 3j, k), which is essentially consistent with *L*-$PheO_n$. Upon extending the *L*-$PheN_n$ chain to $n = 16$, supramolecular chirality disappeared (Fig. 3l), which is in contrast to the restored supramolecular chirality observed in *L*-$PheO_{16}$.

To further investigate the influence of the gelator's hydrophobic tail on the self-assembly process, XRD analysis was employed to elucidate the molecular packing arrangement and predominant driving forces governing gel formation (Fig. 4). Figure 3a, b demonstrate that both *L*-$PheO_n$ and *L*-$PheN_n$ exhibit a distinct broad peak at approximately 19.28°–19.98°, indicating that hydrogen bonds is the primary driving force for the self-assembly of these compounds. A pronounced change was observed in the small-angle X-ray diffraction region upon elongation of the molecular tail chain. The small-angle X-ray diffraction patterns of *L*-$PheO_n$ ($n = 6, 8, 10, 12, 14$) reveal that the interlamellar spacing closely corresponds to the theoretical molecular length,

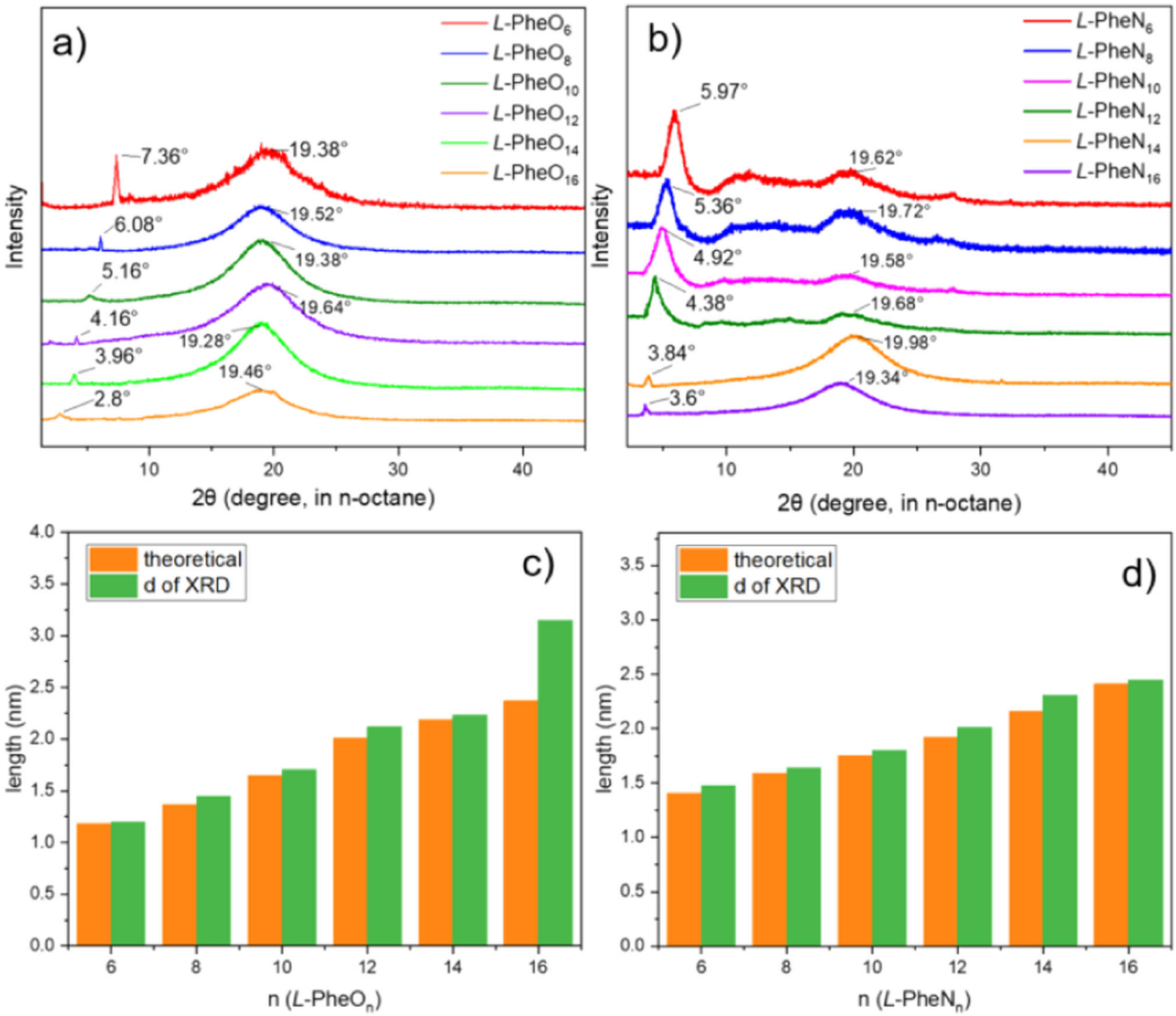

Fig. 4 | XRD spectra and theoretical molecular lengths of organogelators. a *L*-PheO$_n$ in two weakly polar solvents, **b** *L*-PheN$_n$ in two weakly polar solvents, **c** XRD and theoretical molecular lengths of *L*-PheO$_n$, **d** XRD and theoretical molecular lengths of *L*-PheN$_n$.

which indicates the formation of monolayer assemblies in the aggregates. However, when $n = 16$, XRD analysis reveals a marked expansion of the interlayer distance, significantly exceeding the molecular length of organogelators in Fig. 4c. Based on prior evidence[11,46,57], we propose that *L*-PheO$_{16}$ gel likely adopts an interdigitated bilayer stacking, wherein intermolecular hydrogen bonds induce a novel interdigitated bilayer, thereby driving the re-emergence of supramolecular helical chirality. In contrast, the XRD pattern of *L*-PheN$_{16}$ reveals no substantial increase in interlayer distance, with the measured d-value closely corresponding to the molecular dimension of *L*-PheN$_{16}$. The observed difference may arise from the enhanced hydrogen bond network in *L*-PheN$_{16}$, which rendered the van der Waals interactions between alkyl chains and solvents insufficient to disrupt the existing intermolecular hydrogen bonds among gelators[58], thereby preventing the formation of lamellar aggregates observed in *L*-PheO$_{16}$ (Fig. 4d).

Theoretical calculation

Based on XRD characterization results, computational modeling to investigate the supramolecular assembly mechanisms of self-assembly in gels was employed. First, their geometric conformations were optimized using density functional theory (DFT), with the resulting structures depicted in Fig. S16. Among these compounds, *L*-PheO$_n$ exhibits enhanced flexibility in its hydrophobic terminal chains owing to the presence of a single set of intermolecular hydrogen bonds. This structural feature leads to pronounced morphological diversity in the aggregates formed by *L*-PheO$_6$ and *L*-PheO$_{10}$ by xTB[59–61]. Notably, the tail chains of *L*-PheO$_{10}$ demonstrate more compact stacking arrangements compared to the other derivatives (Fig. 5a, b, snapshots from other angles can be found in Fig. S17). In contrast, the aggregates of *L*-PheN$_6$ and *L*-PheN$_{10}$ exhibited minimal structural variation with increasing tail chain length, which can be attributed to the ability of the *L*-PheN$_n$ molecular backbone to form additional intermolecular hydrogen bonds (Fig. 5c, d), which is consistent with the XRD results.

Furthermore, Fig. 5e reveals a distinctive bilayer assembly mechanism in *L*-PheO$_{16}$ gels, wherein the hydrophobic alkyl chains mediate lamellar stacking through van der Waals interactions. Intermolecular hydrogen bonds on both lateral sides generate a novel double-layered architecture, leading to supramolecular helical chirality. In contrast, *L*-PheN$_{16}$ maintains monolayer aggregation behavior as evidenced in Fig. 5f. The mutually restrictive effects between amide-derived hydrogen networks and van der Waals interactions among elongated hydrophobic tail chains effectively suppress supramolecular helical chirality formation in the gels, which prevents the supramolecular chirality regenerated in *L*-PheN$_{16}$ gels as achieved by *L*-PheO$_{16}$.

The influence of achiral factors on supramolecular chiral assembly and chirality inversion was investigated using phenylalanine-based organogels,

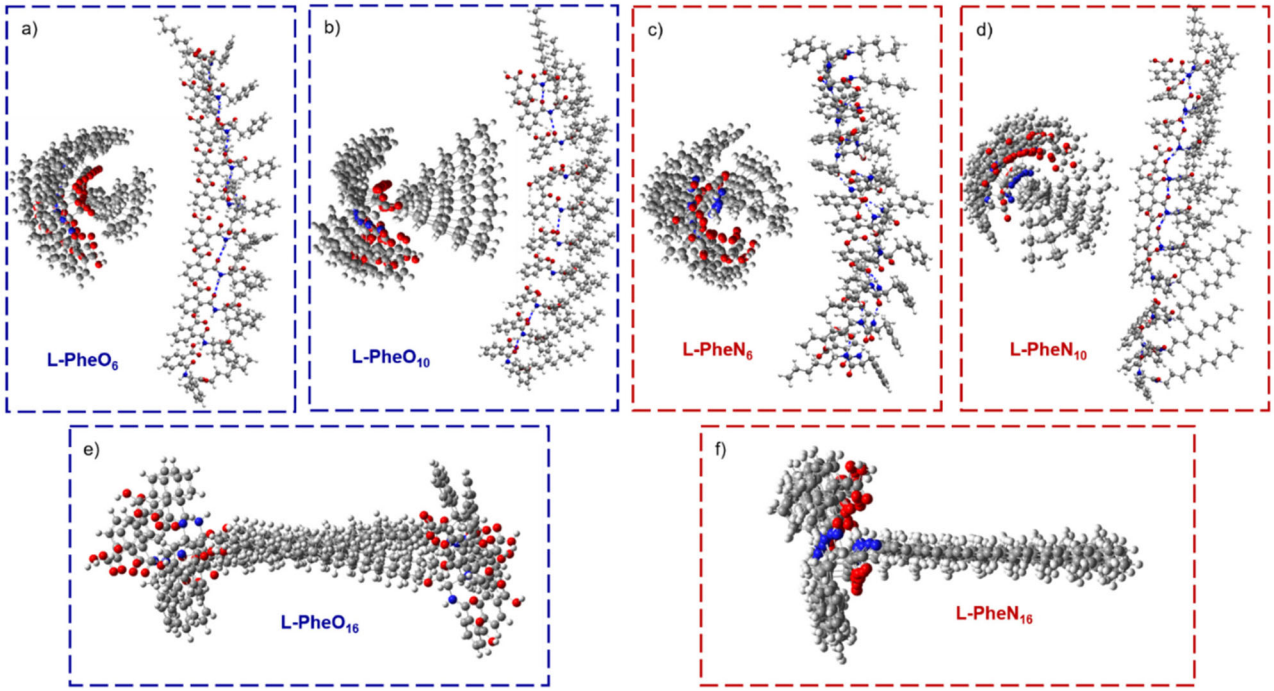

Fig. 5 | Computational simulation of the assembly of *L*-PheN$_n$ and *L*-PheO$_n$ in *n*-octane. **a** *L*-PheO$_6$ with *P*-helix, **b** *L*-PheO$_{10}$ with *P*-helix, **c** *L*-PheN$_6$ with *P*-helix, **d** *L*-PheN$_{10}$ with *P*-helix, **e** *L*-PheO$_{16}$ with *P*-helix. **f** *L*-PheN$_{16}$ with sheet.

enabling precise control over the supramolecular chirality of *L*-PheO$_n$ gels in low-polarity, achiral environments. Subsequently, gelators with enhanced hydrogen bond interactions (*L*-PheN$_n$) were successfully constructed, allowing for a comparative analysis between single-set and multi-set hydrogen bond supramolecular aggregates. These findings unequivocally establish the pivotal role of achiral parameters in regulating supramolecular chirality. To elucidate the mechanistic underpinnings of chiral assembly, molecular simulations were employed to model the supramolecular gel system. Computational results demonstrate that multiple achiral factors, including solvent microenvironment, hydrophobic chain length, and hydrogen bond interactions, significantly modulate the self-assembly behavior of molecular aggregates. This theoretical framework provides critical insights for the rational design of chirality-controllable supramolecular materials.

Methods

Synthesis and characterization of organogels

The synthetic route for the organogelators is shown in Fig. S1, and the detailed synthesis method is described in SI 1.1. For all organogelators, the structures were confirmed using 1H NMR (NMR spectra in SI 1.2). All gels were prepared by "heating-cooling" in alkane solvents, and the gels formed in all solvents were white or translucent, as described in SI 1.3 and Fig. S14. Gels were prepared and tested in XRD, FTIR, and scanning electron microscopy (SEM) using the same concentrations of samples.

Preparation process of organogels

The gelation properties of a series of organogelators in several solvents were characterized. The procedure is to heat a mixture containing a certain amount of organogelator and solvent at 120 °C. When a clear solution was formed, it was stopped and automatically cooled to 25 °C and kept warm. The solution is allowed to stand for 20 min to check for gelation.

Preparation process of xerogel

The prepared organogel was transferred to a silicon plate, and the solvent in the organogel was removed under reduced pressure (0.1 mbar, 25 °C) to obtain a xerogel. We found in the experiment that the variation of temperature affects the microscopic morphology of the xerogel, so 25 °C was used as the standard temperature for this work.

Scanning electron microscopy (SEM)

The xerogels were coated with platinum vapor and analyzed on a Hitachi SU-8010 (SU-8000) microscope operated at 5.0 kV.

X-ray diffraction (XRD) measurements

XRD of gels were analyzed using a Rigaku D/MAX-RB instrument. The X-ray beam generated with a rotating Cu anode at the wavelength of Kα beam at 1.5406 Å was directed toward the film edge and scanning was done up to a 2θ value from 1.5–48°, the scan rate was 4°/min.

Data availability

The authors declare that the data supporting the findings of this study are available and included in the article and its Supplementary Information file. Other detailed experimental procedures are listed in the Supplementary Information file. All data are available from the corresponding author upon request.

Received: 17 May 2025; Accepted: 31 July 2025;
Published online: 12 August 2025

References

1. Ji, J. et al. The more the slower: self-inhibition in supramolecular chirality induction, memory, erasure, and reversion. *J. Am. Chem. Soc.* **144**, 1455–1463 (2022).
2. Guo, Y. et al. Simultaneous chiral fixation and chiral regulation endowed by dynamic covalent bonds. *Angew. Chem. Int. Ed.* **62**, e202312259 (2023).
3. Cheng, Q., Hao, A. & Xing, P. Dynamic evolution of supramolecular chirality manipulated by H-bonded coassembly and photoisomerism. *Mater. Chem. Front.* **5**, 6628–6638 (2021).
4. Sang, Y. et al. Ultrasound-directed symmetry breaking and spin filtering of supramolecular assemblies from only achiral building blocks. *Angew. Chem. Int. Ed.* **62**, e202215867 (2023).

5. Wu, H. et al. Helical self-assembly-induced singlet–triplet emissive switching in a mechanically sensitive system. *J. Am. Chem. Soc.* **139**, 785–791 (2017).
6. Klawa, S. J. et al. Uncovering supramolecular chirality codes for the design of tunable biomaterials. *Nat. Commun.* **15**, 788 (2024).
7. Hirao, T., Kishino, S. & Haino, T. Supramolecular chiral sensing by supramolecular helical polymers. *Chem. Commun.* **59**, 2421–2424 (2023).
8. Zhang, Y. et al. Direct observation of long-range chirality transfer in a self-assembled supramolecular monolayer at interface in situ. *Nat. Commun.* **13**, 7737 (2022).
9. Yang, D., Duan, P., Zhang, L. & Liu, M. Chirality and energy transfer amplified circularly polarized luminescence in composite nanohelix. *Nat. Commun.* **8**, 15727 (2017).
10. Zhao, C. et al. Handedness-inverted and stimuli-responsive circularly polarized luminescent nano/micromaterials through pathway-dependent chiral supramolecular polymorphism. *Adv. Mater.* **36**, 2403329 (2024).
11. Liu, M., Zhang, L. & Wang, T. Supramolecular chirality in self-assembled systems. *Chem. Rev.* **115**, 7304–7397 (2015).
12. Han, X. et al. Chiral induction in covalent organic frameworks. *Nat. Commun.* **9**, 1294 (2018).
13. Jia, S. et al. Chirality supramolecular systems: helical assemblies, structure designs, and functions. *Small* **20**, 2307874 (2023).
14. Xing, P. & Zhao, Y. Controlling supramolecular chirality in multicomponent self-assembled systems. *Acc. Chem. Res.* **51**, 2324–2334 (2018).
15. van der Tol, J. J. B., Vantomme, G., Palmans, A. R. A. & Meijer, E. W. Controlling the processability and stability of supramolecular polymers using the interplay of intra- and intermolecular interactions. *Macromolecules* **55**, 6820–6829 (2022).
16. Wang, Y. et al. Elucidation of the origin of chiral amplification in discrete molecular polyhedra. *Nat. Commun.* **9**, 488 (2018).
17. Liu, G., Humphrey, M. G., Zhang, C. & Zhao, Y. Self-assembled stereomutation with supramolecular chirality inversion. *Chem. Soc. Rev.* **52**, 4443–4487 (2023).
18. Zhang, L. et al. Spiral fractal patterns via hierarchical assembly. *Nano Res.* **15**, 1079–1086 (2021).
19. Zhang, G., Cheng, X., Wang, Y. & Zhang, W. Supramolecular chiral polymeric aggregates: construction and applications. *Aggregate* **4**, e262 (2022).
20. Dou, X. et al. Supramolecular hydrogels with tunable chirality for promising biomedical applications. *Acc. Chem. Res.* **53**, 852–862 (2020).
21. Wang, F., Qiu, H. & Feng, C. Wrapping chiral nanoribbons into coiled and condensed microstructures in supramolecular hydrogels. *Adv. Funct. Mater.* **30**, 2002936 (2020).
22. Wang, S. et al. Chiral helical peptide nanomaterials: construction strategies and applications. *Nano Today* **62**, 102703 (2025).
23. Liang, J., Hao, A., Xing, P. & Zhao, Y. Inverse evolution of helicity from the molecular to the macroscopic level based on N-terminal aromatic amino acids. *ACS Nano* **15**, 5322–5332 (2021).
24. Lee, H.-E. et al. Amino-acid- and peptide-directed synthesis of chiral plasmonic gold nanoparticles. *Nature* **556**, 360–365 (2018).
25. Zheng, R. et al. Assembly of short amphiphilic peptoids into nanohelices with controllable supramolecular chirality. *Nat. Commun.* **15**, 3264 (2024).
26. Liu, G. F., Zhu, L. Y., Ji, W., Feng, C. L. & Wei, Z. X. Inversion of the supramolecular chirality of nanofibrous structures through co-assembly with achiral molecules. *Angew. Chem. Int. Ed.* **55**, 2411–2415 (2015).
27. Geng, Z. et al. Moebius strips of chiral block copolymers. *Nat. Commun.* **10**, 4090 (2019).
28. Liu, G., Liu, J., Feng, C. & Zhao, Y. Unexpected right-handed helical nanostructures co-assembled froml-phenylalanine derivatives and achiral bipyridines. *Chem. Sci.* **8**, 1769–1775 (2017).
29. Wang, F., Qiu, H. & Feng, C. Wrapping chiral nanoribbons into coiled and condensed microstructures in supramolecular hydrogels. *Adv. Funct. Mater.* **556**, 360–365 (2020).
30. Shen, Z., Wang, T. & Liu, M. Macroscopic chirality of supramolecular gels formed from achiral tris(ethyl cinnamate) benzene-1,3,5-tricarboxamides. *Angew. Chem. Int. Ed.* **53**, 13424–13428 (2014).
31. Green, M. M. et al. A helical polymer with a cooperative response to chiral information. *Science* **268**, 1860–1866 (1995).
32. Langeveld-Voss, B. M. W., Waterval, R. J. M., Janssen, R. A. J. & Meijer, E. W. Principles of “Majority Rules” and “Sergeants and Soldiers” applied to the aggregation of optically active polythiophenes: evidence for a multichain phenomenon. *Macromolecules* **32**, 227–230 (1999).
33. Oda, R., Huc, I., Schmutz, M., Candau, S. J. & MacKintosh, F. C. Tuning bilayer twist using chiral counterions. *Nature* **399**, 566–569 (1999).
34. Nonokawa, R. & Yashima, E. Detection and amplification of a small enantiomeric imbalance in α-amino acids by a helical poly(phenylacetylene) with crown ether pendants. *J. Am. Chem. Soc.* **125**, 1278–1283 (2003).
35. Yamamoto, T., Murakami, R., Komatsu, S. & Suginome, M. Chirality-amplifying, dynamic induction of single-handed helix by chiral guests to macromolecular chiral catalysts bearing boronyl pendants as receptor sites. *J. Am. Chem. Soc.* **140**, 3867–3870 (2018).
36. Green, M. M. et al. Macromolecular stereochemistry: the out-of-proportion influence of optically active comonomers on the conformational characteristics of polyisocyanates. The sergeants and soldiers experiment. *J. Am. Chem. Soc.* **111**, 6452–6454 (1989).
37. Palmans, A. R. A., Vekemans, J. A. J. M., Havinga, E. E. & Meijer, E. W. Sergeants-and-soldiers principle in chiral columnar stacks of disc-shaped molecules with C3 symmetry. *Angew. Chem. Int. Ed. Engl.* **36**, 2648–2651 (1997).
38. Markvoort, A. J., ten Eikelder, H. M. M., Hilbers, P. A. J., de Greef, T. F. A. & Meijer, E. W. Theoretical models of nonlinear effects in two-component cooperative supramolecular copolymerizations. *Nat. Commun.* **2**, 509 (2011).
39. Ke, Y.-Z., Nagata, Y., Yamada, T. & Suginome, M. Majority-rules-type helical poly(quinoxaline-2,3-diyl)s as highly efficient chirality-amplification systems for asymmetric catalysis. *Angew. Chem. Int. Ed.* **54**, 9333–9337 (2015).
40. Du, C., Li, Z., Zhu, X., Ouyang, G. & Liu, M. Hierarchically self-assembled homochiral helical microtoroids. *Nat. Nanotechnol.* **17**, 1294–1302 (2022).
41. Cao, Y. et al. Supramolecular meso-trick: ambidextrous mirror symmetry breaking in a liquid crystalline network with tetragonal symmetry. *J. Am. Chem. Soc.* **144**, 6936–6945 (2022).
42. Wang, M. et al. Unexpected role of achiral glycine in determining the suprastructural handedness of peptide nanofibrils. *ACS Nano* **15**, 10328–10341 (2021).
43. Liu, G. et al. Controlling supramolecular chirality of two-component hydrogels by J- and H-aggregation of building blocks. *J. Am. Chem. Soc.* **140**, 6467–6473 (2018).
44. Su, L. et al. Dilution-induced gel-sol-gel-sol transitions by competitive supramolecular pathways in water. *Science* **377**, 213–218 (2022).
45. Shen, Z., Jiang, Y., Wang, T. & Liu, M. Symmetry breaking in the supramolecular gels of an achiral gelator exclusively driven by π–π stacking. *J. Am. Chem. Soc.* **137**, 16109–16115 (2015).
46. Zhu, X. et al. Homochiral nanotubes from heterochiral lipid mixtures: a shorter alkyl chain dominated chiral self-assembly. *Chem. Sci.* **10**, 3873–3880 (2019).

47. Zhu, L. et al. Chirality control for in situ preparation of gold nanoparticle superstructures directed by a coordinatable organogelator. *J. Am. Chem. Soc.* **135**, 9174–9180 (2013).
48. Fu, K., Zhao, Y. & Liu, G. Pathway-directed recyclable chirality inversion of coordinated supramolecular polymers. *Nat. Commun.* **15**, 9571 (2024).
49. Yao, L. et al. Metallophilic interaction-mediated hierarchical assembly and temporal-controlled dynamic chirality inversion of metal–organic supramolecular polymers. *ACS Nano* **17**, 2159–2169 (2023).
50. Mabesoone, M. F. J. et al. Competitive hydrogen bonding in supramolecular polymerizations of tribenzylbenzene-1,3,5-tricarboxamides. *Mol. Syst. Des. Eng.* **5**, 820–828 (2020).
51. Yan, X., Wang, Q., Chen, X. & Jiang, Y. B. Supramolecular chiral aggregates exhibiting nonlinear CD–ee dependence. *Adv. Mater.* **32**, 1905667 (2020).
52. Ślęczkowski, M. L., Mabesoone, M. F. J., Ślęczkowski, P., Palmans, A. R. A. & Meijer, E. W. Competition between chiral solvents and chiral monomers in the helical bias of supramolecular polymers. *Nat. Chem.* **13**, 200–207 (2020).
53. Mondal, A. K. et al. Spin filtering in supramolecular polymers assembled from achiral monomers mediated by chiral solvents. *J. Am. Chem. Soc.* **143**, 7189–7195 (2021).
54. Kar, T., Mandal, S. K. & Das, P. K. Organogel–hydrogel transformation by simple removal or inclusion of N-Boc-protection. *Chemistry***17**, 14952–14961 (2011).
55. Kishimura, A., Yamashita, T. & Aida, T. Phosphorescent organogels via "metallophilic" interactions for reversible RGB−color switching. *J. Am. Chem. Soc.* **127**, 179–183 (2005).
56. Grimme, S. Do special noncovalent π–π stacking interactions really exist?. *Angew. Chem. Int. Ed.* **47**, 3430–3434 (2008).
57. Chen, C., Chen, J., Wang, T. & Liu, M. Fabrication of helical nanoribbon polydiacetylene via supramolecular gelation: circularly polarized luminescence and novel diagnostic chiroptical signals for sensing. *ACS Appl. Mater. Interfaces* **8**, 30608–30615 (2016).
58. Lu, T. & Chen, Q. Visualization analysis of weak interactions in chemical systems. *Comprehensive Computational Chemistry* **2**, 240–264 (2024).
59. Bannwarth, C., Ehlert, S. & Grimme, S. GFN2-xTB—an accurate and broadly parametrized self-consistent tight-binding quantum chemical method with multipole electrostatics and density-dependent dispersion contributions. *J. Chem. Theory Comput.* **15**, 1652–1671 (2019).
60. Bannwarth, C. et al. Extended tight-binding quantum chemistry methods. *WIREs Comput. Mol. Sci.* **11**, e1493 (2021).
61. Grimme, S., Bannwarth, C. & Shushkov, P. A Robust and accurate tight-binding quantum chemical method for structures, vibrational frequencies, and noncovalent interactions of large molecular systems parametrized for all spd-block elements (Z = 1–86). *J. Chem. Theory Comput.* **13**, 1989–2009 (2017).

Acknowledgements

This work was financially supported by the National Natural Science Foundation of China (Grant No. 21978124) and the Natural Science Foundation of Ningbo (Grant Nos. 2024J009 and 2024J139).

Author contributions

Y.-P.H. and F.Y. conceived and designed the experiments. W.Z. carried out the experiments and the computational simulation.

Competing interests

The authors declare no competing interests.

Additional information

Supplementary information The online version contains supplementary material available at https://doi.org/10.1038/s42004-025-01650-8.

Correspondence and requests for materials should be addressed to Yu-Peng He.

Peer review information *Communications Chemistry* thanks the anonymous reviewers for their contribution to the peer review of this work.